Magnetite Thin Films by Solvothermal Synthesis on a Microstructured Si Substrate as a Model to Study Energy Storage Mechanisms of Supercapacitors

Karina Chavez [ID] and Enrique Quiroga-González *[ID]

Institute of Physics, Benemérita Universidad Autónoma de Puebla, Puebla 72570, Mexico;
karichavez269@gmail.com
* Correspondence: equiroga@ieee.org; Tel.: +52-222-2295500 (ext. 2061)

Abstract: Fast electrochemical phenomena occurring in supercapacitors are hard to analyze by ex situ or in situ techniques because many of them are meta-stable (the supercapacitor relaxes once it is not further polarized). In a steady state, one observes the effect of charge storage but not necessarily the mechanism. This is a problem for Raman spectroscopy, too, even though Raman spectra of the electrodes of supercapacitors are commonly recorded ex situ or in a steady state in situ. Raman operando is desired, but it represents a technological challenge since the electrochemical events in a supercapacitor are very fast (occurring within seconds), and in contrast, Raman requires from seconds to minutes to collect enough photons for reliable spectra. This work presents the development of electrodes made of thin layers of iron oxide grown solvothermally on Si wafers, with a porosified surface and resistivity of 0.005 Ωcm, to study their performance as electrodes in supercapacitors and analyze their energy storage mechanisms by cyclic voltammetry and Raman operando. Being flat and containing just iron oxide and silicon, these electrodes allow for studying interfacial phenomena with minor interferents.

Keywords: microstructured Si current collector; iron oxide thin film; energy storage mechanisms; cyclic voltammetry; Raman operando; fast energy storage; supercapacitor

1. Introduction

Developing energy storage systems with higher reliability, higher capacity, higher efficiency, longer lifetime, lower cost, and higher power has been a hot topic for researchers in the last two decades [1]. Particularly, high-power energy storage is of great interest because of the applications demanding it and the challenges of studying it. A supercapacitor (SC) is an energy storage device with unique features such as a high power density, fast charge and discharge rate, long cycle life, and wide working temperature range [2]. Researchers have sought ways to optimize the electrochemical performance of supercapacitors by developing new electrode materials and cell designs [3]. However, as the energy storage mechanism is not fully understood, the further development of these devices is limited.

It is commonly thought that the main energy storage mechanism of supercapacitors is capacitive, directly proportional to the surface area of the active materials. However, many times, the capacity is larger than expected. In such a case, the charge storage may not be limited to the surface of the electrodes but should also be related to redox processes in the shallow bulk of the electrodes (faradaic processes) [4]. When charges are stored in a way that the current is proportional to the change in voltage in time, it seems capacitive; however, if one knows that it is not fully capacitive, as stated before, the mechanism is called pseudocapacitive. So far, it is known that a pseudocapacitive-type redox process occurs over a wide potential range and in a discharge time of seconds–minutes, while a battery-type redox process occurs at a specific potential and in a longer time (minutes–hours) [5]. However, as the processes may occur very shallowly in the bulk

of the electrodes, and they may present metastable phenomena depending on the potential, they are difficult to study. It is not yet well known how the structure or composition of metal oxides are altered while charging/discharging the supercapacitors made of them. The behavior is not entirely clear in the specific case of magnetite (Fe_3O_4). Some authors attribute its storage to a contribution of EDLC and pseudocapacitance, which imply the reduction/oxidation of anions specifically adsorbed on the surface [6,7]. Other authors only attribute its capacitance, at least in part, to a surface redox reaction that depends on the electrolyte used [8,9].

Here, Fe_3O_4 (magnetite) was used in thin layers grown directly on a planar substrate to more clearly observe the processes on the surface. Different methods exist to synthesize Fe_3O_4 nanoparticles, such as ball milling [10], coprecipitation [11], sonochemical methods [12], chemical methods [13,14], and solvothermal methods [15–17]. In this research, the solvothermal route was used because it is a technique that allows the material to be synthesized in a single step; on the other hand, it is a soft chemical technique that offers the possibility of tuning the morphology and size of the particles of the products. However, the focus is on obtaining thin films, and there are just a few reports of solvothermal synthesis of films [18–20]. Particularly, magnetite deposition by the solvothermal route has still not been well studied.

This work aims to elucidate the energy storage mechanisms of supercapacitors of metal oxides by operando Raman spectroscopy. Since there are different theories for electrochemical energy storage mechanisms, which have not been confirmed due to the high speed of the processes, using an operando technique could be the answer. Operando Raman studies could allow for the analysis of the intermediate compounds and of the surface reactions of the electrode with the electrolyte. Fe_3O_4 was selected to be studied in this work as an example, considering that it is a typical material for anionic storage. For this purpose, Fe_3O_4 nanoparticles were grown on a Si wafer with a porosified surface and resistivity of 0.005 Ωcm by solvothermal synthesis without the use of any additives (conductive additive or binder). The porous surface offered nucleation spots for the growth of the Fe_3O_4 nanoparticles, which have the shape of nano-walls. To the best of the knowledge of the authors, there are no previous reports on operando Raman spectroscopy of magnetite supercapacitors.

2. Materials and Methods

2.1. Fe_3O_4 Electrode Synthesis

Iron (II, III) oxide was prepared using as a precursor an iron (III) chloride hexahydrate (sigma-aldrich 98%) at 0.12 M, sodium acetate (sigma-aldrich 99%) at 1.2 M as an electrostatic agent to control the particle growth from attracting each other, and ethylene glycol anhydrous (sigma-aldrich 99.8%) as a high boiling point reducing agent. The mixture was stirred for 30 min at room temperature to obtain a well-dispersed solution before transferring into a hydrothermal Teflon reactor. The synthesis conditions were 12 h at 195 °C, just like other investigations, to produce iron oxides [21,22]. However, the difference in the present work is that magnetite was deposited on a textured Si chip (of 1 cm^2). For this, the chip was introduced in the Teflon reactor before adding the mother solution. After the synthesis, the sample was recovered by magnetic separation. Afterward, repetitive washes were performed with ethanol and water. Then, the sample was allowed to dry under vacuum. The final product was a uniform film of magnetite with 0.0163 g weight on the textured substrate.

2.2. Silicon Substrate Treatment

A p-type silicon wafer (1-0-0) chip with a 0.001–0.005 Ωcm resistivity and thickness of 500 $\pm$ 10 μm was treated with a 4:4:32 (V:V:V) etching solution of $HF:H_2O_2:H_2O$ for 10 min at 40 °C. These conditions have effectively achieved texturization of the silicon wafer [23], aiming to obtain nanometric nucleation points for the deposition of iron oxide.

2.3. Characterization

X-ray diffractometry was performed with a Panalytical-Empyrean diffractometer to identify the solids formed after the solvothermal process. A Horiba LabRAM Raman microscope (Minami-ku, Kyoto, Japan) with a He-Ne laser (632.8 nm) was used for chemical and structural analysis. The morphology of the samples was observed by scanning electron microscopy (SEM) with a JSM-7800F (Jeol, Akishima, Tokyo, Japan). Cyclic voltammetry was performed using a Zennium Zahner potentiostat (Kronach, Germany). For this, an electrochemical cell with three electrodes was used. The counter electrode was platinum, with Ag/AgCl as a reference electrode, and the iron oxide was deposited on a Si chip as a working electrode. Measurements were made using 1 M sodium sulfate (Na_2SO_4) or 3 M potassium chloride (KCl) as electrolytes at scanning rates of 2–200 mV/s.

3. Results and Discussion

The diffractogram of the powder product without substrate (Figure 1) shows peaks located at angular positions of 18.4°, 24.8°, 30.2°, 35.6°, 37.4°, 43.3°, 53.7°, 57.2°, 62.8°, 71.4°, 74.2°, 75.6°, and 79.3° 2θ indexed to the planes (111), (211), (220), (311), (222), (400), (422), (511), (440), (620), (533), (622), and (444) of Fe_3O_4 (magnetite), which has a cubic structure with space group Fd-3m (JCPDS #100-6668) [24]. Using the Debye–Scherrer equation [25] and measuring the FWHM of the (311) peak, the crystallite size was determined to be 18.5 nm. No characteristic peaks of other iron oxides were observed in the XRD pattern.
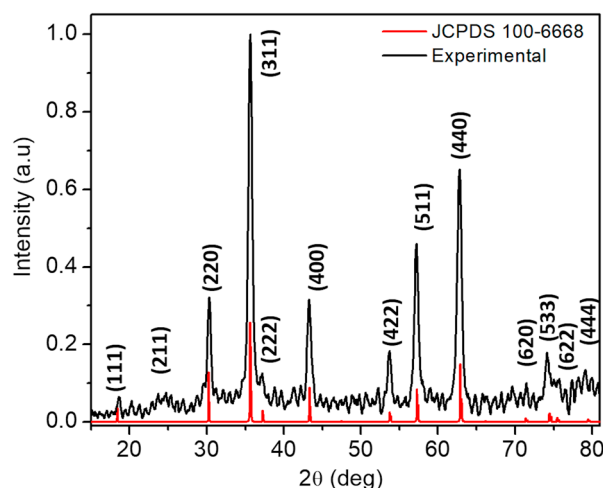

**Figure 1.** XRD pattern of Fe_3O_4 synthesized via a solvothermal route.

Raman spectra were recorded to confirm the presence of magnetite. Figure 2 illustrates the spectrum for the iron oxide film deposited on the silicon wafer, which showed three prominent bands at 310, 460, 530, and 666 cm^{-1} associated with the vibration modes E_g, T_{2g}, T_{2g}, and A_{1g} of magnetite [26]. All bands can be attributed to Fe-O lattice vibrations. Furthermore, the A_{1g} band is broad and prominent, as is characteristic of magnetite [27].

Figure 3 shows SEM micrographs of the silicon chip coated with iron oxide. This technique corroborates that iron oxide is obtained in nanometric size. One can conclude that by carrying out a single-step synthesis process, the nanostructures can be deposited on a Si current collector to be used as an electrode in a supercapacitor. Figure 3a is a micrograph of a chemically treated Si chip; it can be seen that pores of about 55 nm are formed and are evenly distributed on the Si surface. Figure 3b,c show micrographs that indicate that a uniform coating of iron oxide particles is deposited on the Si substrate. The particles have a nano-wall shape. Such a large-surface-area shape is promissory for enhanced electrochemical performance [28]. The growth and distribution of the iron oxide particles coincide with the size and distribution of the nanopores in the silicon wafer. This

indicates that the pores at the surface of the Si chip served as a nucleation point for the iron oxide, influencing its size and shape.
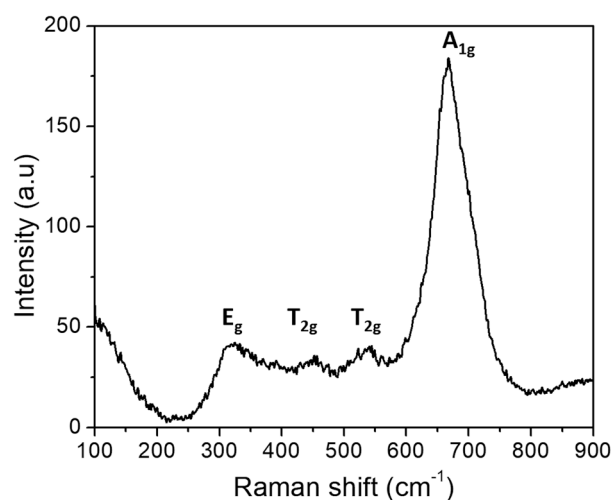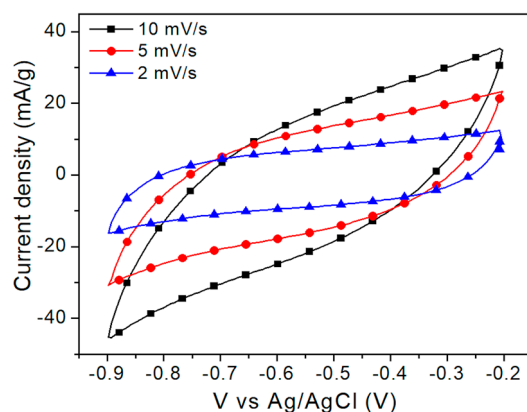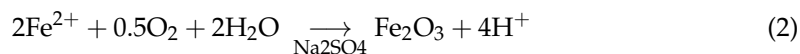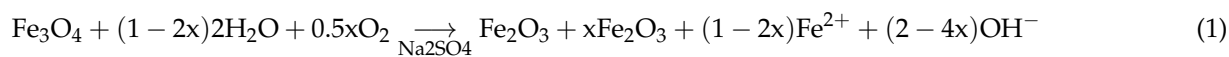

**Figure 2.** Raman spectrum of Fe_3O_4 on a textured silicon chip.
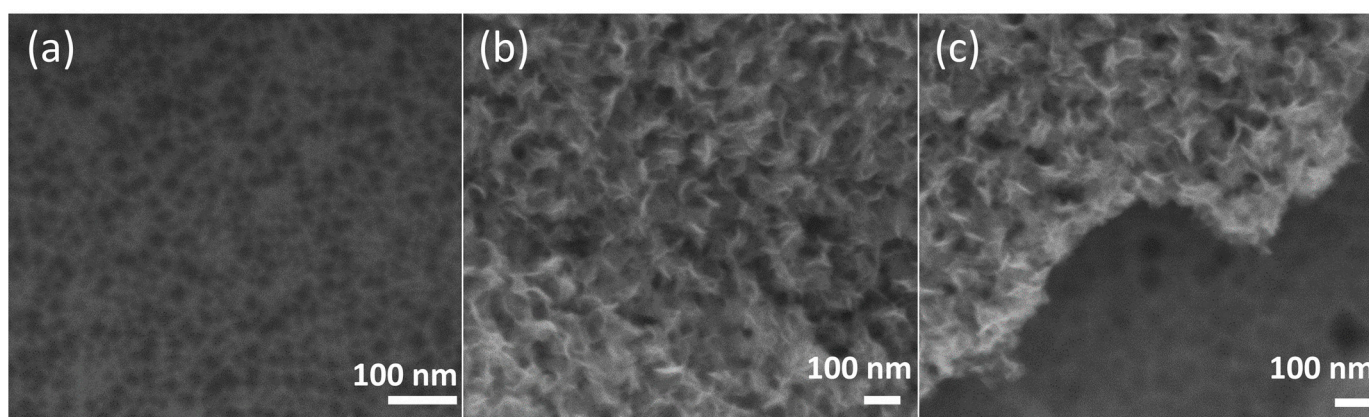
Figure 3. SEM micrographs of (**a**) the porosified silicon chip and of (**b**,**c**) the Fe_3O_4 film.

Cyclic voltammetry tests were performed using a three-electrode cell to determine the iron oxide processes when used as a supercapacitor's electrode. Figure 4 shows the voltammograms belonging to the Fe_3O_4 films in a Na_2SO_4 [1 M] aqueous solution at the rates of 2, 5, and 10 mVs^{-1} in a potential window of -0.9 to -0.2 V. An increase in the width of the graphs when increasing the rates and a well-defined rectangular shape can be attributed to the simultaneous occurrence of faradaic and non-faradaic processes to store energy [29]. At higher rates (Figure S1), a large ohmic contribution to the total current can be observed (the slope of the curves is large).

The thin films used as electrodes in a supercapacitor were analyzed by ex situ Raman before and after cyclic voltammetry. After being cycled with the Na_2SO_4 electrolyte, considerable differences were found when compared with the pristine sample. In Figure 5, one can see that in the Raman spectrum, besides the Fe_3O_4 bands, bands corresponding to the hematite phase (α-Fe_2O_3) appear at positions 220, 240, 305, and 610 cm^{-1} [30]. The additional bands at 520 and 992 cm^{-1} correspond to Si and Na_2SO_4, respectively. The result indicates that magnetite was oxidized to hematite when using an electrolyte with a high oxygen content, such as Na_2SO_4, during cyclic voltammetry. It has been shown that the oxygen in an aqueous solution is unable to turn magnetite into hematite. However, adding an oxidant triggers the oxidation reaction [31]. Na_2SO_4 works as an oxidant to form hematite, as described in Equations (1) and (2) [31]:

$$Fe_3O_4 + (1 - 2x)2H_2O + 0.5xO_2 \xrightarrow[\text{Na2SO4}]{} Fe_2O_3 + xFe_2O_3 + (1 - 2x)Fe^{2+} + (2 - 4x)OH^- \tag{1}$$

$$2Fe^{2+} + 0.5O_2 + 2H_2O \xrightarrow[\text{Na2SO4}]{} Fe_2O_3 + 4H^+ \tag{2}$$

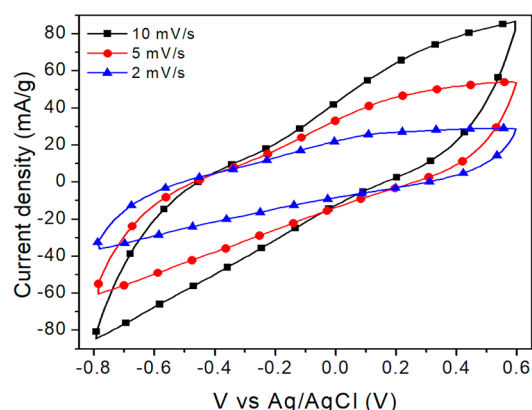**Figure 4.** Cyclic voltammetry of the Fe_3O_4 substrates in Na_2SO_4 at different scan rates.
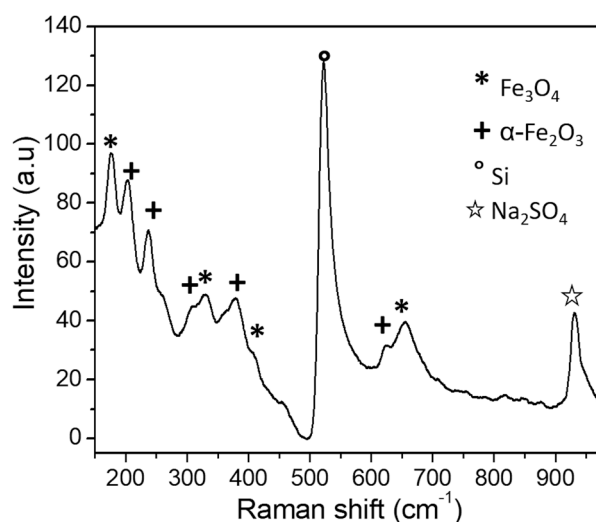
Figure 5. Ex situ Raman spectrum of the Fe_3O_4 film after the CV cycles in [1 M] Na_2SO_4.

Considering that magnetite is oxidized to hematite in Na_2SO_4, cyclic voltammetry was then performed using 3 M KCl as an electrolyte. We decided to change the electrolyte to one that does not contain oxygen in its structure to avoid the oxidation of magnetite. KCl has already been used in supercapacitors in the range of −0.1 to 0.7 V, avoiding oxidation [32]. It is known that the presence of oxygen-containing functional groups favors the oxidation of mixed oxides such as magnetite [33]. In this work, we tried to avoid the oxidation of magnetite to hematite because the capacitances reported for hematite are much lower (~190 F/g) [34,35] than those of Fe_3O_4, which are around 500/600 F/g [8,36,37].

Figure 6 shows the voltammetric responses obtained at different scan rates from 2 mVs^{-1} to 10 mVs^{-1}. In all cases, the potential sweep initiates negatively concerning the zero-current potential. It is observed that at slower scanning rates, the electrode's response as a supercapacitor is better. A semi-rectangular shape is observed, but a faradaic peak can be observed even at rates as high as 10 mV/s at about 0.15 V. The electrochemical performance of the electrodes highly depends on the physicochemical properties of the electrolyte, such as molar conductivity and ionic mobility [38]. The current density observed

with KCl is larger than with Na_2SO_4, probably due to the higher ionic conductivity of the KCl solution (probably because it has a higher concentration).

Figure 6. Cyclic voltammetry of the Fe_3O_4 substrates in KCl at different scan rates.

Fe_3O_4 is known as an anion-storing electrode for supercapacitors. As KCl is a salt that readily dissociates in water, the Cl^- anions could be adsorbed and desorbed on the surface of the Fe_3O_4 particles, being responsible for the capacitance and pseudocapacitance. Physisorption and desorption of Cl^- are not exactly reversible, or they have different velocities, so the CV curves were not found to be symmetrical, which is in agreement with previous studies [39,40].

Ex situ Raman was used to analyze the supercapacitor electrodes before and after cycling using a KCl electrolyte, as shown in Figure 7. In this case, the spectrum did not change significantly, and no bands corresponding to other iron oxides appeared. The predominant bands observed were those of magnetite at 670, 530, and 310 cm^{-1}. This makes KCl a good candidate for analyzing the storage mechanism of Fe_3O_4 in an electrochemical supercapacitor.
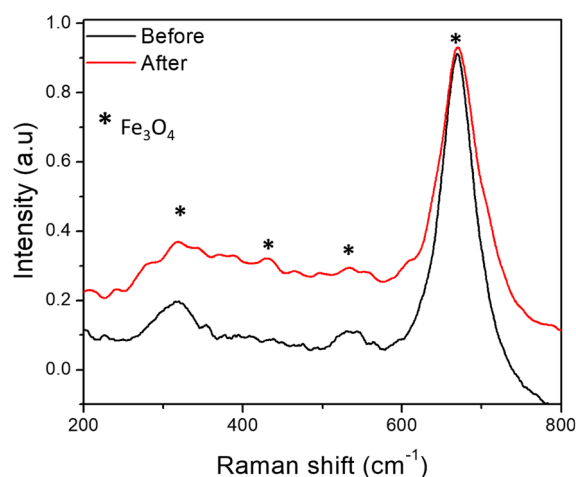
Figure 7. Ex situ Raman spectra of Fe_3O_4 film before and after the CV cycles in [3 M] KCl.

To calculate the capacitance of the supercapacitor assembly being evaluated, Equation (3) was used, which describes the typical relaxation time (τ) of a capacitor with capacitance *C* in parallel with a resistor with resistance *R*. Any real capacitor presents conduction current, whose existence can be modeled with *R*. The values of τ and could be obtained from the current components that can be observed in the voltammogram of Figure 8. The exponential line represents mainly a capacitive current (i_c) since it is at least one order of magnitude larger than the ohmic current in the marked current section. By fitting that curve section with Equation (4) and changing the x-axis by time, τ can be calculated. Here, *t* is the time,

and i_0 is the current at time $t = 0$. This fit is correct if performed at voltages at which redox contributions to the current are minimum (where no peaks are observed). Finally, the linear line represents an ohmic current (i_R), from which the resistance can be obtained with Equation (5), where V is the voltage and $\frac{\Delta V}{\Delta i_R}$ is the inverse of the discrete derivative of the curve. The whole data treatment to determine the C of a supercapacitor can, from now on, be known as Quiroga's method.

$$\tau = RC \tag{3}$$

$$i_c = i_0 e^{\frac{-t}{\tau}} \tag{4}$$

$$R = \frac{\Delta V}{\Delta i_R} \tag{5}$$
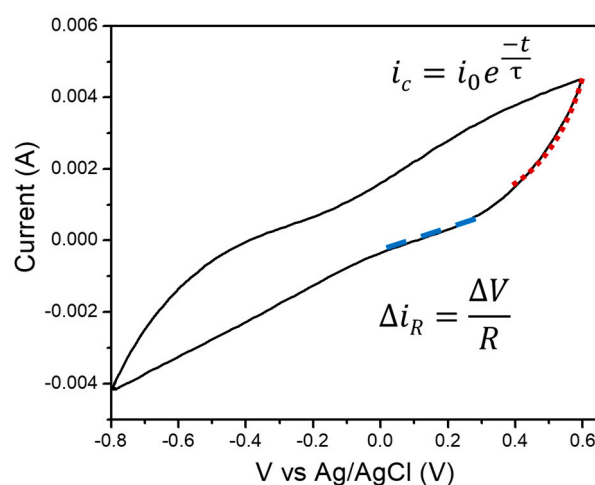
Figure 8. Typical cyclic voltammogram indicating the different components of the observed current.

Table 1 illustrates the behavior of capacitance, resistance, and relaxation time as a function of the scan rate of the analyzed sample in KCl. The capacitance at high scan rates has an almost constant tendency, which can be attributed to the fact that the capacitive component of the supercapacitor does not respond correctly due to the concentration of the electrolyte (Figure S2). This material's activity as a supercapacitor is generally analyzed at rates lower than 20 mVs^{-1} since the response is not linearly proportional to the scan rate compared to an ideal capacitor [41]. As the scan rates decrease, it can be observed that the capacitance is larger and relatively constant. On the other hand, the resistance and the relaxation time increase. Since the resistance of the solution and the electrode can distort the response of the current at the switching potential, and this distortion depends on the scan rate, the shape of the curves changes when increasing the scan rate [42].

Table 1. Capacitance, resistance, and relaxation time values as a function of the scan rate.

Scan Rate [V/s]	R [Ω]	τ [s]	C [F]	C [F/g]
0.002	881.05727	45.79298	0.05198	16.65866
0.005	505.61798	22.94127	0.04537	14.54254
0.01	321.94598	14.39368	0.04471	14.32961
0.02	242.71845	9.96214	0.04104	13.15513
0.05	271.96653	6.22587	0.02289	7.33719
0.1	240.32043	4.2858	0.01783	5.71593
0.2	283.28612	2.6158	0.00923	2.95954

To gain insight into the storage mechanism of iron oxide thin films used as electrodes in a supercapacitor, we analyzed the capacitive (i_{cap}) and diffusive (i_{dif}) currents using Equation (6), where *Vel* is the voltage sweep rate and K_{dif} is the diffusion coefficient. This equation is a modification of Dunn's equation, typically used to explain the energy storage mechanisms in supercapacitors, but incorporating the ohmic current. To know about the diffusion and capacitive currents, the ohmic current must be first eliminated. The premise of the existence of the ohmic current is the base of Quiroga's method. The results are condensed in Table 2 for the current at about 0.15 V (where a redox peak is observed). It can be observed that at voltage scan rates up to 50 mVs^{-1}, charge storage is diffusion-limited ($i_{cap}/i_{dif} < 1$), despite the capacitance being relatively constant in that voltage scan rate range. Supercapacitors are commonly planned to have a high capacitive or pseudocapacitive response, looking for high power density [43,44]. When the process is limited by diffusion, as in the present case, the charge/discharge rates are constrained, and also the power density obtained [45,46].

$$i = i_R + i_{cap} + i_{dif} = i_R + C\ Vel + K_{dif} Vel^{\frac{1}{2}} \qquad (6)$$

Table 2. Capacitive and diffusive current and their relationship as a function of scanning rate.

| Scan Rate [V/s]	$C = \tau/R$ [F]	i_{cap}	i_{dif}	i_{cap}/i_{dif}
0.002	0.05198	1.04×10^{-4}	7.42×10^{-4}	0.1401
0.005	0.04537	2.27×10^{-4}	0.00109	0.20898
0.01	0.04471	4.47×10^{-4}	0.00134	0.33273
0.02	0.04104	8.21×10^{-4}	0.00125	0.65907
0.05	0.02289	0.00114	0.00156	0.73582
0.1	0.01783	0.00178	7.93×10^{-4}	2.24978
0.2	0.00923	0.00185	9.69×10^{-4}	1.90594

Under experimental conditions, magnetite is easily prone to oxidation when exposed to heat or humidity. In fact, during the measurement of the Raman scattering spectra, the cell assembly with the Fe_3O_4 electrode was exposed to the environment for several hours, which led to the sample being slightly oxidized before being measured in the operating Raman. In the oxidation of magnetite, the crystal size is a crucial factor in determining oxidation kinetics and, therefore, different oxidation mechanisms [47]. For tiny crystals (less than 300 nm), an intermediate phase, maghemite (γ-Fe_2O_3), is produced before the final product, hematite (α-Fe_2O_3), is formed [48].

The iron oxide-based electrode was characterized by means of operando Raman spectroscopy. There are some works on operando Raman spectroscopy of some metal oxides and 2D materials [49–51], especially studying batteries [52,53]; however, there are no previous reports on operando Raman of Fe_3O_4 electrodes in a supercapacitor. Applying the technique to the study of supercapacitors could be complicated due to the short-time processes occurring and the long time needed to acquire a good number of counts by Raman. In this work, the study of magnetite electrodes was enabled by growing them as a thin film directly on an inert substrate without using any additives or binders that could mask certain phenomena.

Raman spectra were recorded while performing cyclic voltammetry in the range of -0.8 to 0.6 V at a rate of 5 mVs^{-1}. The band at 490 cm^{-1}, corresponding to the γ-Fe_2O_3 (maghemite) phase [54], is the one that suffers the largest changes, as can be observed in Figure 9. No apparent changes could be observed in other bands (see Figure S3). As a shoulder at about 510 cm^{-1}, it is possible to identify Fe_3O_4 (magnetite) [18]. Interestingly, as the voltage goes to positive values, the band moves towards maghemite, while it moves towards magnetite when going back to negative values. A vertical dashed line is drawn in Figure 9 in order to easily observe this shift. The observed phenomenon can be explained

in the following way: when the voltages go positive, the chlorine ions are attracted to the surface of the electrode, and they cannot only form a double-layer electrochemical capacitor but they can also be allocated inside the iron oxides, as elucidated from the voltammetry tests. Such an effect has been observed in studies of chlorinated water in iron pipes. In the presence of chlorine, ferrous oxides are transformed into ferric oxides, and the residual chlorine is consumed in the process [55]. Actually, Fe is partially in ferrous form (2+) in magnetite, and it is in ferric form (3+) in maghemite. The shift may be enhanced due to the stress induced by the incorporation of chlorine. It is known that when there is tensile stress (as occurs when introducing chlorine into the structure), there is a red shift of the Raman bands, and when there is compressive stress (as occurs when releasing chlorine), there is a blue shift [56]. It is remarkable that the process is reversible in the present study.
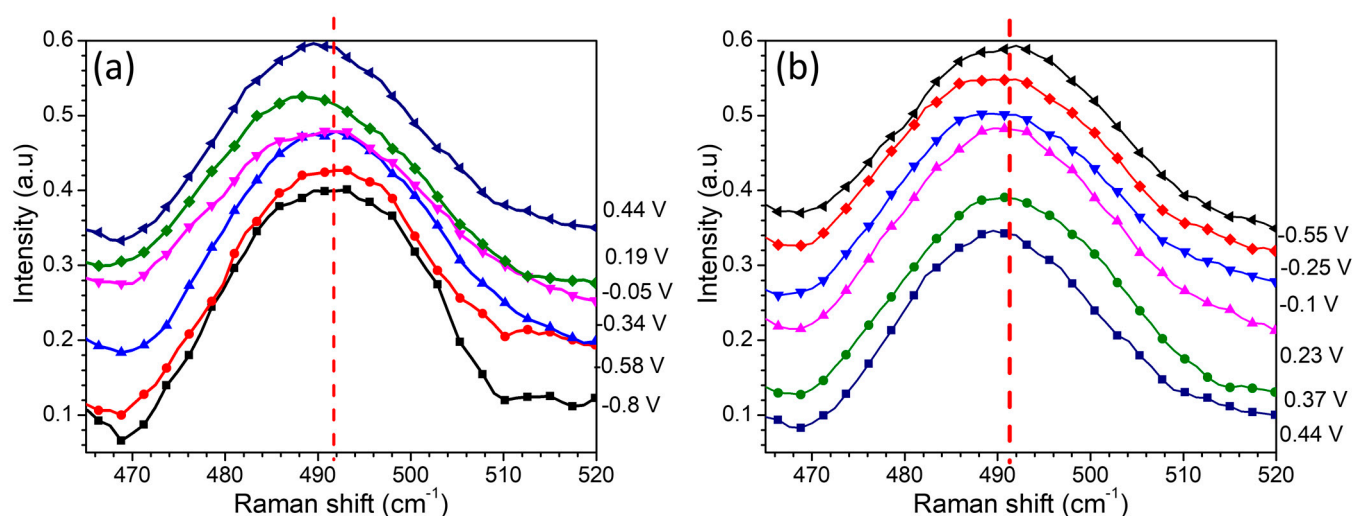
Figure 9. Raman operando spectra of Fe_3O_4 film (**a**) charge and (**b**) discharge in [3 M] KCl.

4. Conclusions

Using the solvothermal method and Si substrates with a porosified surface, it has been possible to deposit thin films of Fe_3O_4. These samples have been used as model electrodes of supercapacitors to study interfacial phenomena by voltammetry and operando Raman. It has been observed that diffusion-limited processes dominate energy storage, even at voltage scan rates of 50 mVs^{-1}, despite the capacitance being relatively constant. This process could be related to chlorine incorporation into Fe_3O_4, causing its oxidation to γ-Fe_2O_3. At much larger voltage scan rates, energy storage is mainly capacitive despite it being low. This study may represent the first one on operando Raman of Fe_3O_4, electrodes in a supercapacitor, and one of the first ones on operando Raman of supercapacitors in general. The developed methodology can be applied to other fast electrochemical systems. The formation of meta-stable compounds, as has been evidenced in the present study, is complicated by any ex situ techniques.

Author Contributions: K.C.: writing—original draft preparation, investigation, and methodology; E.Q.-G.: conceptualization, formal analysis, data curation, writing—review and editing, supervision, and resources. All authors have read and agreed to the published version of the manuscript.

Data Availability Statement: The original contributions presented in this study are included in this article/Supplementary Materials. Further inquiries can be directed to the corresponding author/s.

Conflicts of Interest: The authors declare no conflicts of interest.

References

1. Sayed, E.T.; Olabi, A.G.; Alami, A.H.; Radwan, A.; Mdallal, A.; Rezk, A.; Abdelkareem, M.A. Renewable energy and energy storage systems. *Energies* **2023**, *16*, 1415. [CrossRef]
2. Devillers, N.; Jemei, S.; Péra, M.-C.; Bienaimé, D.; Gustin, F. Review of characterization methods for supercapacitor modelling. *J. Power Sources* **2014**, *246*, 596–608. [CrossRef]
3. Attia, S.Y.; Mohamed, S.G.; Barakat, Y.F.; Hassan, H.H.; Zoubi, W.A. Supercapacitor electrode materials: Addressing challenges in mechanism and charge storage. *Rev. Inorg. Chem.* **2022**, *42*, 53–88. [CrossRef]
4. Okwundu, O.S.; Ugwuoke, C.O.; Okaro, A.C. Recent trends in non-faradaic supercapacitor electrode materials. *Metall. Mater. Eng.* **2019**, *25*, 105–138. [CrossRef] [PubMed]
5. Kuo, S.-L.; Lee, J.-F.; Wu, N.-L. Study on pseudocapacitance mechanism of aqueous $MnFe_2O_4$ supercapacitor. *J. Electrochem. Soc.* **2006**, *154*, A34. [CrossRef]
6. Aghazadeh, M.; Karimzadeh, I.; Ganjali, M.R. Electrochemical evaluation of the performance of cathodically grown ultra-fine magnetite nanoparticles as electrode material for supercapacitor applications. *J. Mater. Sci. Mater. Electron.* **2017**, *28*, 13532–13539. [CrossRef]
7. Wang, S.-Y.; Ho, K.-C.; Kuo, S.-L.; Wu, N.-L. Investigation on Capacitance Mechanisms of Fe_3O_4 Electrochemical Capacitors. *J. Electrochem. Soc.* **2006**, *153*, A75. [CrossRef]
8. Wu, N.-L.; Wang, S.-Y.; Han, C.-Y.; Wu, D.-S.; Shiue, L.-R. Electrochemical capacitor of magnetite in aqueous electrolytes. *J. Power Sources* **2003**, *113*, 173–178. [CrossRef]
9. Tipsawat, P.; Wongpratat, U.; Phumying, S.; Chanlek, N.; Chokprasombat, K.; Maensiri, S. Magnetite (Fe_3O_4) nanoparticles: Synthesis, characterization and electrochemical properties. *Appl. Surf. Sci.* **2018**, *446*, 287–292. [CrossRef]
10. Li, Y.; Zimmerman, A.R.; He, F.; Chen, J.; Han, L.; Chen, H.; Hu, X.; Gao, B. Solvent-free synthesis of magnetic biochar and activated carbon through ball-mill extrusion with Fe_3O_4 nanoparticles for enhancing adsorption of methylene blue. *Sci. Total Environ.* **2020**, *722*, 137972. [CrossRef] [PubMed]
11. Nkurikiyimfura, I.; Wang, Y.; Safari, B.; Nshingabigwi, E. Temperature-dependent magnetic properties of magnetite nanoparticles synthesized via coprecipitation method. *J. Alloys Compd.* **2020**, *846*, 156344. [CrossRef]
12. Fuentes-García, J.s.A.; Carvalho Alavarse, A.; Moreno Maldonado, A.C.; Toro-Córdova, A.; Ibarra, M.R.; Goya, G.F.n. Simple sonochemical method to optimize the heating efficiency of magnetic nanoparticles for magnetic fluid hyperthermia. *ACS Omega* **2020**, *5*, 26357–26364. [CrossRef] [PubMed]
13. Mylkie, K.; Nowak, P.; Rybczynski, P.; Ziegler-Borowska, M. Polymer-Coated Magnetite Nanoparticles for Protein Immobilization. *Materials* **2021**, *14*, 248. [CrossRef] [PubMed]
14. Chala, G.H.; Zeleke, T.D. Green synthesis of magnetite nanoparticles using Catha edulis plant leaf extract for removal of hexavalent Chromium from aqueous solution. *Int. J. Nano Dimens.* **2023**, *14*, 73–90.
15. Liang, Y.; Jiang, L.; Xu, S.; Ju, W.; Tao, Z.; Yang, Y.; Peng, X.; Wei, G. Synthesis and Characterization of Fe_3O_4 Nanoparticles Prepared by Solvothermal Method. *J. Mater. Eng. Perform.* **2024**, *33*, 6804–6815. [CrossRef]
16. Shaterabadi, Z.; Delgado, Á.; Iglesias, G.R. Solvothermally synthesized magnetite nanorods for application in magnetic hyperthermia and photothermia. *J. Magn. Magn. Mater.* **2024**, *596*, 171990. [CrossRef]
17. Sahadevan, J.; Sojiya, R.; Padmanathan, N.; Kulathuraan, K.; Shalini, M.; Sivaprakash, P.; Muthu, S.E. Magnetic property of Fe_2O_3 and Fe_3O_4 nanoparticle prepared by solvothermal process. *Mater. Today Proc.* **2022**, *58*, 895–897. [CrossRef]
18. Zhan, Y.; Zhao, R.; Meng, F.; Lei, Y.; Zhong, J.; Yang, X.; Liu, X. Oriented growth of magnetite along the carbon nanotubes via covalently bonded method in a simple solvothermal system. *Mater. Sci. Eng. B* **2011**, *176*, 779–784. [CrossRef]
19. Ma, J.; Liu, W.; Zhang, S.; Zhao, J.; Li, W. One-step solvothermal approach for preparing soft magnetic hydrophilic PFR coated Fe3O4 nanocrystals. *J. Alloys Compd.* **2011**, *509*, 7895–7899. [CrossRef]
20. Zhu, H.; Yang, D.; Zhu, L. Hydrothermal growth and characterization of magnetite (Fe_3O_4) thin films. *Surf. Coat. Technol.* **2007**, *201*, 5870–5874. [CrossRef]
21. Ooi, F.; DuChene, J.S.; Qiu, J.; Graham, J.O.; Engelhard, M.H.; Cao, G.; Gai, Z.; Wei, W. *A Facile Solvothermal Synthesis of Octahedral Fe_3O_4 Nanoparticles*; Pacific Northwest National Laboratory (PNNL): Richland, WA, USA, 2015.
22. Li, S.; Zhang, T.; Tang, R.; Qiu, H.; Wang, C.; Zhou, Z. Solvothermal synthesis and characterization of monodisperse superparamagnetic iron oxide nanoparticles. *J. Magn. Magn. Mater.* **2015**, *379*, 226–231. [CrossRef]
23. Aca-López, V.; Quiroga-González, E.; Gómez-Barojas, E.; Światowska, J.; Luna-López, J.A. Effects of the doping level in the production of silicon nanowalls by metal assisted chemical etching. *Mater. Sci. Semicond. Process.* **2020**, *118*, 105206. [CrossRef]
24. Raja, K.; Verma, S.; Karmakar, S.; Kar, S.; Das, S.J.; Bartwal, K. Synthesis and characterization of magnetite nanocrystals. *Cryst. Res. Technol.* **2011**, *46*, 497–500. [CrossRef]
25. Hall, B.; Zanchet, D.; Ugarte, D. Estimating nanoparticle size from diffraction measurements. *J. Appl. Crystallogr.* **2000**, *33*, 1335–1341. [CrossRef]

26. Shebanova, O.N.; Lazor, P. Raman spectroscopic study of magnetite (FeFe$_2$O$_4$): A new assignment for the vibrational spectrum. *J. Solid State Chem.* **2003**, *174*, 424–430. [CrossRef]

27. Shebanova, O.N.; Lazor, P. Raman study of magnetite (Fe$_3$O$_4$): Laser-induced thermal effects and oxidation. *J. Raman Spectrosc.* **2003**, *34*, 845–852. [CrossRef]

28. Zeng, X.; Yang, B.; Li, X.; Li, R.; Yu, R. Solvothermal synthesis of hollow Fe$_3$O$_4$ sub-micron spheres and their enhanced electrochemical properties for supercapacitors. *Mater. Des.* **2016**, *101*, 35–43. [CrossRef]

29. Sinan, N.; Unur, E. Fe$_3$O$_4$/carbon nanocomposite: Investigation of capacitive & magnetic properties for supercapacitor applications. *Mater. Chem. Phys.* **2016**, *183*, 571–579. [CrossRef]

30. Dar, M.I.; Shivashankar, S. Single crystalline magnetite, maghemite, and hematite nanoparticles with rich coercivity. *RSC Adv.* **2014**, *4*, 4105–4113. [CrossRef]

31. Zhao, J.; Brugger, J.; Pring, A. Mechanism and kinetics of hydrothermal replacement of magnetite by hematite. *Geosci. Front.* **2019**, *10*, 29–41. [CrossRef]

32. Patil, S.M.; Shingte, S.R.; Karade, V.C.; Kim, J.H.; Kulkarni, R.M.; Chougale, A.D.; Patil, P.B. Electrochemical performance of magnetic nanoparticle-decorated reduced graphene oxide (MRGO) in various aqueous electrolyte solutions. *J. Solid State Electrochem.* **2021**, *25*, 927–938. [CrossRef]

33. Tang, J.; Myers, M.; Bosnick, K.A.; Brus, L.E. Magnetite Fe3O4 Nanocrystals: Spectroscopic Observation of Aqueous Oxidation Kinetics. *J. Phys. Chem. B* **2003**, *107*, 7501–7506. [CrossRef]

34. Shivakumara, S.; Penki, T.R.; Munichandraiah, N. Preparation and electrochemical performance of porous hematite (α-Fe$_2$O$_3$) nanostructures as supercapacitor electrode material. *J. Solid State Electrochem.* **2014**, *18*, 1057–1066. [CrossRef]

35. Wang, D.; Wang, Q.; Wang, T. Controlled synthesis of mesoporous hematite nanostructures and their application as electrochemical capacitor electrodes. *Nanotechnology* **2011**, *22*, 135604. [CrossRef] [PubMed]

36. Sanei, A.; Irani, M.A.; Kolvari, E.; Koukabi, N.; Dashtian, K. Unveiling magnetite metal-organic frameworks for asymmetric pseudo-supercapacitor with high energy density and magnetocapacitance. *J. Energy Storage* **2024**, *100*, 113759. [CrossRef]

37. Cheng, J.P.; Shou, Q.L.; Wu, J.S.; Liu, F.; Dravid, V.P.; Zhang, X.B. Influence of component content on the capacitance of magnetite/reduced graphene oxide composite. *J. Electroanal. Chem.* **2013**, *698*, 1–8. [CrossRef]

38. Zhang, X.; Wang, X.; Jiang, L.; Wu, H.; Wu, C.; Su, J. Effect of aqueous electrolytes on the electrochemical behaviors of supercapacitors based on hierarchically porous carbons. *J. Power Sources* **2012**, *216*, 290–296. [CrossRef]

39. Thakur, A.V.; Lokhande, B.J. Electrolytic anion affected charge storage mechanisms of Fe$_3$O$_4$ flexible thin film electrode in KCl and KOH: A comparative study by cyclic voltammetry and galvanostatic charge–discharge. *J. Mater. Sci. Mater. Electron.* **2017**, *28*, 11755–11761. [CrossRef]

40. Choudhury, B.J.; Moholkar, V.S. Magnetite–Graphene-Based Composites and Their Potential Application as Supercapacitor Electrode Material. In *Handbook of Magnetic Hybrid Nanoalloys and their Nanocomposites*; Thomas, S., Rezazadeh Nochehdehi, A., Eds.; Springer International Publishing: Cham, Switzerland, 2022; pp. 879–914.

41. Chen, J.; Huang, K.; Liu, S. Hydrothermal preparation of octadecahedron Fe$_3$O$_4$ thin film for use in an electrochemical supercapacitor. *Electrochim. Acta* **2009**, *55*, 1–5. [CrossRef]

42. O'Neill, L.; Johnston, C.; Grant, P.S. Enhancing the supercapacitor behaviour of novel Fe$_3$O$_4$/FeOOH nanowire hybrid electrodes in aqueous electrolytes. *J. Power Sources* **2015**, *274*, 907–915. [CrossRef]

43. Choi, C.; Ashby, D.S.; Butts, D.M.; DeBlock, R.H.; Wei, Q.; Lau, J.; Dunn, B. Achieving high energy density and high power density with pseudocapacitive materials. *Nat. Rev. Mater.* **2020**, *5*, 5–19. [CrossRef]

44. An, C.; Zhang, Y.; Guo, H.; Wang, Y. Metal oxide-based supercapacitors: Progress and prospectives. *Nanoscale Adv.* **2019**, *1*, 4644–4658. [CrossRef]

45. Eftekhari, A. Surface Diffusion and Adsorption in Supercapacitors. *ACS Sustain. Chem. Eng.* **2019**, *7*, 3692–3701. [CrossRef]

46. Johns, P.A.; Roberts, M.R.; Wakizaka, Y.; Sanders, J.H.; Owen, J.R. How the electrolyte limits fast discharge in nanostructured batteries and supercapacitors. *Electrochem. Commun.* **2009**, *11*, 2089–2092. [CrossRef]

47. Feitknecht, W.; Gallagher, K.J. Mechanisms for the Oxidation of Fe$_3$O$_4$. *Nature* **1970**, *228*, 548–549. [CrossRef] [PubMed]

48. Guo, C.; Hu, Y.; Qian, H.; Ning, J.; Xu, S. Magnetite (Fe$_3$O$_4$) tetrakaidecahedral microcrystals: Synthesis, characterization, and micro-Raman study. *Mater. Charact.* **2011**, *62*, 148–151. [CrossRef]

49. Chen, D.; Ding, D.; Li, X.; Waller, G.H.; Xiong, X.; El-Sayed, M.A.; Liu, M. Probing the Charge Storage Mechanism of a Pseudocapacitive MnO2 Electrode Using in Operando Raman Spectroscopy. *Chem. Mater.* **2015**, *27*, 6608–6619. [CrossRef]

50. Meng, C.; Das, P.; Shi, X.; Fu, Q.; Müllen, K.; Wu, Z.-S. In Situ and Operando Characterizations of 2D Materials in Electrochemical Energy Storage Devices. *Small Sci.* **2021**, *1*, 2000076. [CrossRef]

51. Gupta, S.; Carrizosa, S.B.; Jasinski, J.; Dimakis, N. Charge transfer dynamical processes at graphene-transition metal oxides/electrolyte interface for energy storage: Insights from in-situ Raman spectroelectrochemistry. *AIP Adv.* **2018**, *8*, 065225. [CrossRef]

52. Flores, E.; Novák, P.; Berg, E.J. In situ and Operando Raman Spectroscopy of Layered Transition Metal Oxides for Li-ion Battery Cathodes. *Front. Energy Res.* **2018**, *6*, 82. [CrossRef]

53. Xue, L.; Li, Y.; Hu, A.; Zhou, M.; Chen, W.; Lei, T.; Yan, Y.; Huang, J.; Yang, C.; Wang, X. In Situ/operando Raman techniques in lithium–sulfur batteries. *Small Struct.* **2022**, *3*, 2100170. [CrossRef]

54. Li, G.; Lan, J.; Li, G. Chrysanthemum-like 3D hierarchical magnetic γ-Fe_2O_3 and Fe_3O_4 superstructures: Facile synthesis and application in adsorption of organic pollutants from water. *RSC Adv.* **2015**, *5*, 1705–1711. [CrossRef]
55. Naser, A.M.; Higgins, E.M.; Arman, S.; Ercumen, A.; Ashraf, S.; Das, K.K.; Rahman, M.; Luby, S.P.; Unicomb, L. Effect of groundwater iron on residual chlorine in water treated with sodium dichloroisocyanurate tablets in rural Bangladesh. *Am. J. Trop. Med. Hyg.* **2018**, *98*, 977. [CrossRef] [PubMed]
56. Tuschel, D. Stress, strain, and Raman spectroscopy. *Spectroscopy* **2019**, *34*, 10–21.
57. Kumar, P.; No-Lee, H.; Kumar, R. Synthesis of phase pure iron oxide polymorphs thin films and their enhanced magnetic properties. *J. Mater. Sci. Mater. Electron.* **2014**, *25*, 4553–4561. [CrossRef]